AGU PUBLICATIONS

JGR

Journal of Geophysical Research: Oceans

RESEARCH ARTICLE

10.1002/2016JC011771

Key Points:
- Both bulk and size-fractionated a_{254} significantly correlated with meteoric water fraction indicating that CDOM was terrestrial-dominated
- Large colloids (>100 kDa) mainly occurred in the Chukchi Shelf, while the small (1–10 kDa) and medium colloids (10–100 kDa) were higher in slope and basin waters
- The remote sensing model might underestimate terrestrial DOM input due to its overestimated $s_{275-295}$

Correspondence to:
M. Chen,
mchen@xmu.edu.cn

Citation:
Lin, H., M. Chen, J. Zeng, Q. Li, R. Jia, X. Sun, M. Zheng, and Y. Qiu (2016), Size characteristics of chromophoric dissolved organic matter in the Chukchi Sea, *J. Geophys. Res. Oceans*, *121*, doi:10.1002/2016JC011771.

Received 4 MAR 2016
Accepted 4 AUG 2016
Accepted article online 8 AUG 2016

Size characteristics of chromophoric dissolved organic matter in the Chukchi Sea

Hui Lin[1], Min Chen[1,2], Jian Zeng[1], Qi Li[1], Renming Jia[1], Xiuwu Sun[3], Minfang Zheng[1], and Yusheng Qiu[1]

[1]College of Ocean and Earth Sciences, Xiamen University, Xiamen, China, [2]State Key Laboratory of Marine Environmental Science, Xiamen University, Xiamen, China, [3]Third Institute of Oceanography, State Oceanic Administration, Xiamen, China

Abstract With the Arctic warming, terrestrial input plays a more important role in carbon cycle in the Arctic Ocean than before. Chromophoric dissolved organic matter (CDOM) as a tracer of terrestrial dissolved organic matter (tDOM) becomes more valuable in elucidating the source and compositions of DOM. Although measurements of DOM in the Arctic Ocean have been widely reported, characteristics of high molecular weight colloids are still poorly understood. In this study, the bulk absorbance and size fractograms of CDOM were measured in the Chukchi Seas using an asymmetrical flow field-flow fractionation (AF4) coupled online with UV-vis detectors. Both CDOM a_{254}, absorption coefficient at 254 nm, and the integrated UV_{254} (from AF4 UV-vis detector) of three colloidal fractions (1–10, 10–100, and >100 kDa) significantly correlated with the fraction of meteoric water (f_{mw}) calculated from $\delta^{18}O$ in seawater, which indicates that the CDOM was mainly derived from terrestrial input and a_{254} is a potential tracer of tDOM in the Chukchi Sea. Compared with the larger colloidal fractions (10–100 and >100 kDa), the smaller colloidal fraction (1–10 kDa) showed a stronger correlation with the f_{mw}, suggesting the smaller colloids were of mostly terrigenous origin. Values of field measured spectral slope at 275–295 nm ($s_{275-295}$), a tDOM proxy, were significantly lower than the model-estimated $s_{275-295}$ calculated from the MODIS Aqu satellite remote sensing data, which indicated that terrestrial input of CDOM derived from model calculation was likely underestimated in the Chukchi Sea.

1. Introduction

The Arctic Ocean comprises ~1% of the global ocean volume but receives approximately 10% of the global fluvial discharge, which contributes 12–24% of dissolved organic matter (DOM) mostly in the upper layer of the Arctic Ocean [*Guay et al.*, 1999; *Benner et al.*, 2005; *Amon et al.*, 2012]. This disproportionally high fluvial input makes the terrestrial matter important in marine biogeochemistry in the Arctic Ocean. Recent time series observations revealed a 50% increase in terrestrial particles into the western Arctic Ocean with increasing freshwater discharge, especially over the last decade due to global warming [*Doxaran et al.*, 2015]. Enhanced freshwater discharge and the induced increase of terrestrial input into the Arctic Ocean may have impacts on biogeochemical processes and carbon cycle, which needs to be better understood.

Chromophoric dissolved organic matter (CDOM), which absorbs potentially harmful ultraviolet-visible (UV-vis) radiation, is an important constituent of DOM pool. The CDOM optical absorption reflects both effects of hydrological and biogeochemical processes in marine environments [*Coble*, 2007; *Coble et al.*, 2014]. As one of the most abundant components of CDOM, terrestrial DOM (tDOM) has been quantified and qualified by several indicators in the Arctic Ocean [*Stedmon and Markager*, 2001; *Walker et al.*, 2009; *Fichot et al.*, 2013]. For example, using radionuclides (i.e., radium and ^{14}C [*Benner*, 2004; *Hansell et al.*, 2004; *Letscher et al.*, 2011]) and stable isotopes (i.e., ^{18}O, ^{13}C, and ^{15}N [*Benner et al.*, 2005; *Stedmon et al.*, 2011; *Granskog et al.*, 2012]), the source and fate of tDOM have been studied. However, there are still many unconquered questions need to be solved. The tight linkage between the CDOM absorption coefficient and the fraction of meteoric water observed in the eastern Arctic Ocean suggests its conservative mixing behavior and indicates the terrestrial input as the main source of CDOM [*Granskog et al.*, 2012]. Surprisingly, there have been no reports so far to explore this relationship in the western Arctic Ocean, which has high riverine input [*Stedmon et al.*, 2011].

Field flow fractionation (FFF), a chromatography-like separation technique, was first described by *Giddings et al*. [1976]. Separation and fractionation of particles take place in a ribbon-like channel where an application field is conducted. The macromolecules and colloids are separated according to their abilities of interaction with the field. A variety of fields, such as electronic field and magnetic field, have been applied to this technique [*Schimpf*, 2005]. The flow field which is a cross flow perpendicular to the direction of the channel flow controls fractionation and separation of colloids by their differences in diffusion coefficients. Taking advantages of aquatic solution as a carrier, asymmetric flow field-flow fractionation (AF4) where the cross-flow rate is not vertically equal in the channel profile depicts the size spectrum of artificial nanoparticles and natural colloids [*Giddings et al*., 1976; *Wahlund and Giddings*, 1987; *Giddings*, 1993, 1995; *Dubascoux et al*., 2008]. AF4 is recently applied to study characteristics and compositions of natural colloids in aquatic environments [*Baalousha et al*., 2011; *Jackson et al*., 2015] although its applications to seawater are still few. Using the flow field-flow fractionation combined with inductively coupled plasma mass spectrometry, *Saito et al*. [2015] compares the optical properties and metal compositions of different size colloids in groundwaters. The characteristics and compositions of chromophoric colloidal organic matter in river and coastal seawater have also been reported [*Stolpe et al*., 2010, 2013; *Guéguen et al*., 2013; *Mangal and Guéguen*, 2015; *Zhou and Guo*, 2015]. *Zhou et al*. [2016] and *Stolpe et al*. [2014] reveal the differences of size and compositions between the humic-like and protein-like colloids in the northern Gulf of Mexico.

Here we used the AF4 coupled with UV-vis absorbance detector to first characterize the size-fractionated CDOM optical properties in the Arctic Ocean. Our major objectives were (1) to characterize the size distribution of CDOM and the partitioning of CDOM among different size fractionated colloidal fractions in the Chukchi Sea and (2) to explore the relationship between CDOM a_{254} and the fraction of meteoric water to examine the source of CDOM and the role of tDOM in both the Chukchi Shelf and eastern Chukchi Sea.

2. Methods

2.1. Sampling

Seawater samples for the measurements of CDOM, dissolved organic carbon (DOC), and stable oxygen isotope ($\delta^{18}O$) were collected aboard the R/V *Xuelong* icebreaker during the 6th Chinese Arctic Research Expedition (21 July to 24 September 2014) along two transects: Section R in the Chukchi Shelf and Section S in the eastern Chukchi Sea (Figure 1). The southern stations along the Section R (R1–R9) were located just east of 170°W, from the Bering Strait to the northern Chukchi Shelf, while the northern stations (R11–R15) were located over the Chukchi Plateau. Section S, located in the eastern Chukchi Sea, was from the Barrow Cape to the Beaufort Sea. Sampling covered the whole water column and samples at 3000 m depth were collected at stations R15 and S08. Temperature and salinity were measured using independent CTD sensors mounted on the CTD rosette.

For DOC, CDOM, and AF4 measurements, samples were prefiltered through precombusted GF/F filters (400°C, 0.7 μm, Whatman). Filter holders were connected using an acid-washed, DOC-free silicon tubing. A new filter was loaded prior to each sample filtration to avoid contamination from previous sample.

Samples for stable oxygen isotope were collected using the approach described by *Chen et al*. [2008]. Briefly, seawater was collected directly from a 12 L Niskin bottle into a 30 mL acid-rinsed polyethylene bottle, which was rinsed three times before collection. Caps closed tightly and sealed with parafilm. No bubble should be observed in the sampling bottle. The samples were labeled and stored in ambient temperature before analysis.

2.2. Optical Properties of CDOM

An aliquot of filtrate was collected into a 60 mL acid-cleaned (soaked in 1 M HCl for 24 h) and precombusted (450°C for 5 h) amber borosilicate glass vial for CDOM measurements. CDOM samples were stored in darkness at 4°C until analysis. The absorption spectrum was scanned triply at the range from 240 to 800 nm using a Shimadzu UV2450 spectrophotometer. Absorption coefficient (a) at specific wavelength (e.g., a_{254}), commonly used as an indicator of CDOM concentration, was calculated with the following equation: $a_\lambda = 2.303 * A_\lambda / l$, where the λ is the wavelength, A is the absorbance at a specific wavelength, and l is the length of cuvette. CDOM characteristics were evaluated using the exponential slope of their spectra between 275 and 295 nm ($s_{275-295}$), which has been demonstrated to be a proxy for sources of CDOM

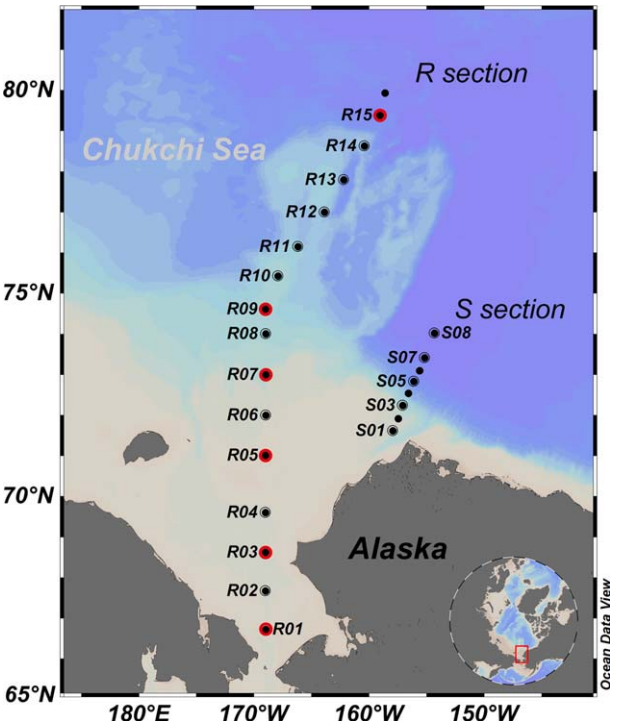

Figure 1. The sampling locations in the Chukchi Seas. All stations including Section R located at the Chukchi Sea and Section S located at the eastern Chukchi Sea are denoted by black points. Note that samples for size separation of colloids by the AF4 were collected at only six stations denoted by black dots with red-edge. The red box in the inserted map indicates our study areas in the Arctic Ocean.

[*Fichot and Benner*, 2012; *Fichot et al.*, 2013]. The spectral slope was calculated with the following equation: $a_\lambda = a_{\lambda_0} e^{S(\lambda-\lambda_0)}$, where a_λ is the absorption coefficient at the wavelength of λ, $a_{\lambda 0}$ is the absorption coefficient at 280 nm, S is the UV-visible spectral slope of samples, and λ is the wavelength. A nonlinear regression by curve fitting toolbox (ctool) was used to fit the exponential curve in MATLAB 7.8.0.347 R2009a software (MathWorks). Modeled $s_{275-295}$ was calculated using the model proposed by *Fichot and Benner* [2012] with the high-resolution (4 km) remote sensing level-3 monthly averaged products downloaded from http://ocean-color.gsfc.nasa.gov/cms/. The time period and locations corresponding with our in situ observation were used. They are from July to August 2014 and 65°N to ~80°N, 150°W to ~180°W, respectively. The selected products were used for model calculation of $s_{275-295}$ in Matlab software. The modeled $s_{275-295}$ from the same location was picked up from the grid database. The specific UV absorbance at 254 nm ($SUVA_{254}$) was derived from DOC-normalized absorbance ($SUVA_{254} = a_{254}$/[DOC]). The $SUVA_{254}$ was proposed to be a reliable proxy for terrigenous DOM, owing to its strong correlation with DOM aromaticity [*Weishaar et al.*, 2003].

2.3. DOC Measurements

DOC samples were collected into a 120 mL preconditioned and acid-washed HDPE bottle (Nalgene, USA) immediately after filtration, and stored at −20°C in dark. DOC was measured by the high-temperature combustion method using a total organic carbon analyzer (Shimadzu TOC-V_{CPH}). A series of potassium hydrogen phthalate (PHP) solutions were used as working standard solutions and measured every six samples to ensure the data quality. The blank using the 18.2 MΩ ultrapure water was generally less than 6 μmol/L. The precision was better than 2% and an accuracy was within 1% based on DOC working standards [*Dai et al.*, 2012].

2.4. Size Fractogram of Colloids

A stirred cell ultrafiltration unit was used to preconcentrate colloidal fractions of DOM for subsequent size analysis by our AF4 system. Ultrafiltration was conducted on board within 1 week after samples were collected and prefiltered (<0.7 μm). The filtrates were stored in a dark and cold (4°C) depository. Approximately 4 L prefiltered seawater was concentrated on board using a UHP-150 stirred cell (Advantec MFS Inc.) equipped with a 1 kDa regenerated cellulose membrane (Millipore PLAC 150 mm diameter) and pressurized by ultrapure nitrogen (0.3–0.4 atm). In order to avoid intercontamination between samples, the cell and membrane were rinsed sequentially with 0.1 M NaOH, 0.1 M HCl, and ultrapure water (18.2 MΩ). The permeate, denoted as the low molecular weight (LMW) fraction, was collected in a 60 mL precombusted (450°C for 5 h) amber borosilicate glass vial and a 120 mL HDPE (Nalgene) bottle for CDOM and DOC measurements, respectively. The retentate, denoted as the high molecular weight (HMW) fraction, was concentrated to approximate 120 mL, and then collected in two 60 mL amber glass vials and stored at 4°C in dark. The mass recovery of DOC during ultrafiltration was determined using concentrations of the bulk DOC (DOC_B), retentate (DOC_R), and integrated permeate (DOC_P) as following equation: $\text{Recovery}(\%) = \frac{\frac{DOC_R - DOC_P}{CF} + DOC_P}{DOC_B} \times 100\%$. The mass recovery of DOC during

Table 1. Experimental Conditions for Size Fractionation of Colloids by the Asymmetrical Field Flow Field Fractionation (AF2000)

Parameters	Value
Accumulation wall membrane	1 kDa polyether sulfone (Postnova)
Carrier solution	0.9% NaCl (aq)
pH value for carrier solution	7.0
Sample injection volume (μL)	628.78
Cross flow (mL min^{-1})	3.5
Channel out flow (mL min^{-1})	0.5
Focus flow (mL min^{-1})	3.8
Focus time (min)	10
Run time (min)	18

ultrafiltration by our stirred cell was determined as 94 ± 2% (Avg ± SD). The >1 kDa HMW colloidal fraction comprises 38 ± 1% of the initial DOC in the Chukchi Sea, which is comparable to previous reports (45%) [*Guo et al*., 1994].

Size fractogram of the HMW fraction was measured on our AF4 system (AF2000 MT, Postnova Analytics, Germany) equipped with a 1 kDa polyether sulfone ultrafiltration membrane (Postnova), coupled with a UV-vis detector (Shimadzu, SPD-M20A) and a fluorescence detector (Shimadzu, RF-20A). AF4 analyses were conducted immediately after ultrafiltered seawater samples were returned to our lab and were completed within 1 month. Six-hundred microliter of retentate solution was injected triply into the AF4 system with a 5 mL glass syringe to obtain three colloidal size spectra. The average M_p and its standard deviation (SD), shown in Table 4, were calculated from the three size spectra. NaCl solution (reagent grade, Sigma-Aldrich) was used as carrier solution and the ionic strength was adjusted to the range of natural seawater. Conditions for the AF4 measurements are summarized in Table 1.

The elution time of natural colloids during AF4 fractionation was calibrated using six globular macromolecules prepared in the carrier solution, including Vitamin-B12, Ribonuclease A type I-A form, Lysozyme, Ovalbumin, and BSA (all from Sigma-Aldrich), with molecular weights (MWs) of 1.33, 13.7, 14.4, 45.0, and 66.0 kDa, respectively. Regression between binary log (log-log) of retention time and MW was performed and used as a calibration line for the calculation of molecular weights of natural colloids (Figure 2a). For comparisons with previous studies, the calibration line between hydrodynamic diameters and MW was also constructed and depicted in Figure 2b [*Stolpe et al*., 2010; *Baalousha et al*., 2011; *Zhou and Guo*, 2015]. Since a_{254} was often used as an indicator of CDOM concentration in previous studies [*Chen et al*., 2004; *Stolpe et al*., 2010], integrated UV absorbance at 254 nm was used to characterize natural colloids here. The signal of the UV absorbance was converted into UV absorption using the following equation: $UV_{254}=2.303*A_{254}/l$, where A is the absorbance at 254 nm and l is path length of the inert flow cell. Integration for the UV absorption peaks was carried out from the void peak to the end of elution. The baseline of fractogram was set using the average data during focus period and final rinse period.

2.5. Stable Oxygen Isotope Analysis and Freshwater Component Calculation

Oxygen isotopic abundance ($\delta^{18}O$) in seawater was measured on a water isotope analyzer (Picarro L2140-i, USA) following the procedure described previously [*Steig et al*., 2014]. The precision of oxygen isotope analysis (in the convention of δ notation) was better than $\pm 0.03‰$ relative to Vienna Standard Mean Ocean Water (VSMOW).

The freshwater components in seawater were calculated from a three end-member mixing model by $\delta^{18}O$ and salinity data [*Chen et al*., 2008]. Briefly, the percentage (%) of each freshwater component was derived from the following mass balance equations:

$$\begin{cases} f_{mw}+f_{sim}+f_{CBDW}=1 \\ f_{mw}\delta_{mw}+f_{sim}\delta_{sim}+f_{CBDW}\delta_{CBDW}=\delta \\ f_{mw}S_{mw}+f_{sim}S_{sim}+f_{CBDW}S_{CBDW}=S \end{cases}$$

where f_{mw}, f_{sim}, and f_{CBDW} are the fractions of meteoric water (combination of river runoff, glacier ice-melt water, and precipitation), sea-ice melted water, and Canada Basin Deep Water (CBDW), respectively; δ_{mw}, δ_{sim}, δ_{CBDW} S_{mw}, S_{sim}, and S_{CBDW} are the corresponding $\delta^{18}O$ values and/or salinities; δ and S are the measured $\delta^{18}O$ and salinity of samples. The end-member values of $\delta^{18}O$ and salinity assessed for the CBDW, meteoric water, and sea-ice melted water were given in Table 2 with data from *Tong* [2014].

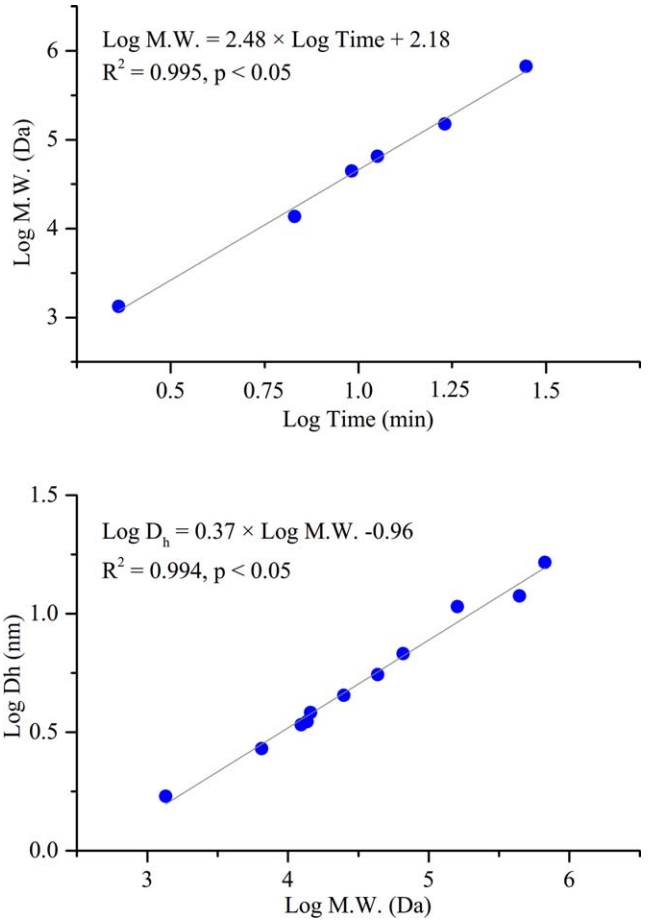

Figure 2. Standardization line for calibration of molecular weights (MW, kDa) and hydrodynamic diameters (D_h, nm) of different size colloids separated by the AF4. We present the binary logistic regression between (a) retention time and MW and the binary logistic regression (b) between the hydrodynamic diameters and the MW. The macromolecules for calibration included vitamin-B12 (1.33 kDa), ribonuclease A type I-A form (13.7 kDa), lysozyme (14.4 kDa), ovalbumin (45.0 kDa), and BSA (66.0 kDa).

3. Results

3.1. CDOM in the Chukchi Shelf (Section R)

Surface water temperature over the Chukchi Shelf (Section R) was as high as 10°C, while the cold seawater with temperature <0°C dominated the depth of 50–300 m in the Chukchi slope beyond 71°N (Figure 3a). The low salinity was observed in the surface water, and the robust halocline was clearly shaped at a depth of 20–50 m along this south-north section (Figure 3b).

The well-mixed shelf water was derived from the northward Bering Shelf Water (BSW) and the low salinity fluvial inputs from boreal rivers. The strong northward flow drove the shelf water with terrestrial materials from the Chukchi shelf to the basin along the isopycnic surface [*Weingartner et al.*, 2005]. The percentages of the meteoric water, sea-ice melted water, and CBDW along this section, calculated from the three end-member mixing model, are shown in Figures 3c–3e. The CBDW with high f_{CBDW} dominated the deep water column and the meteoric water occurred in the upper water column over the basin and slope regions (Figures 3d and 3e). The f_{mw} values were low (5–10%) over the shelf and 20% north of 72.5°N, showing an inverse distribution pattern with that of $\delta^{18}O$ values (Figures 3d and 3f). This agreed well with earlier observations on the distribution of meteoric water in the Chukchi Shelf in 2003 and 2008 summer [*Tong*, 2014]. In addition, positive values of f_{sim} were observed in the shelf region, which represented the net melting of sea ice, while negative values of f_{sim} existed below the depth of 200 m likely induced by the injection of brine.

Coincided with the f_{mw} maximum (Figure 3d) and the f_{sim} minimum (Figure 3e), the high a_{254} values were observed in the halocline of the entire transect (Figure 3g). The high CDOM values agree with previous results which showed a maximal CDOM fluorescence between 40 and 200 m in this area [*Guéguen et al.*, 2007]. Three absorption coefficients at different wavelengths (e.g., a_{254}, a_{280}, and a_{355}) correlated with each other significantly ($P < 0.05$) and have almost the same distribution patterns along the transect (data not shown). Insignificant correlation between a_{254} and DOC was observed in Section R. However, in the slope and basin areas, DOC and a_{254} had a significant correlation ($R^2 = 0.312$, $P < 0.01$), although this relationship was not observed in the Chukchi shelf ($R^2 = 0.156$, $P > 0.01$). The $SUVA_{254}$ values were high in surface waters of the

Table 2. The End-Member Values of Salinity and $\delta^{18}O$ for the Meteoric Water, Sea-Ice Melted Water, and Canada Basin Deep Water (CBDW) in the Chukchi Seas

End-Member	Salinity	$\delta^{18}O$ (‰)	References
Meteoric water	0	−20.0 ± 2	*Ekwurzel et al.* [2001], *Chen et al.* [2003], and *Bauch et al.* [2011]
Sea-ice melted water	4.0 ± 1.0	−2.0 ± 0.1	*Ekwurzel et al.* [2001]
CBDW	35.0 ± 0.05	0.3 ± 0.1	*Ekwurzel et al.* [2001]

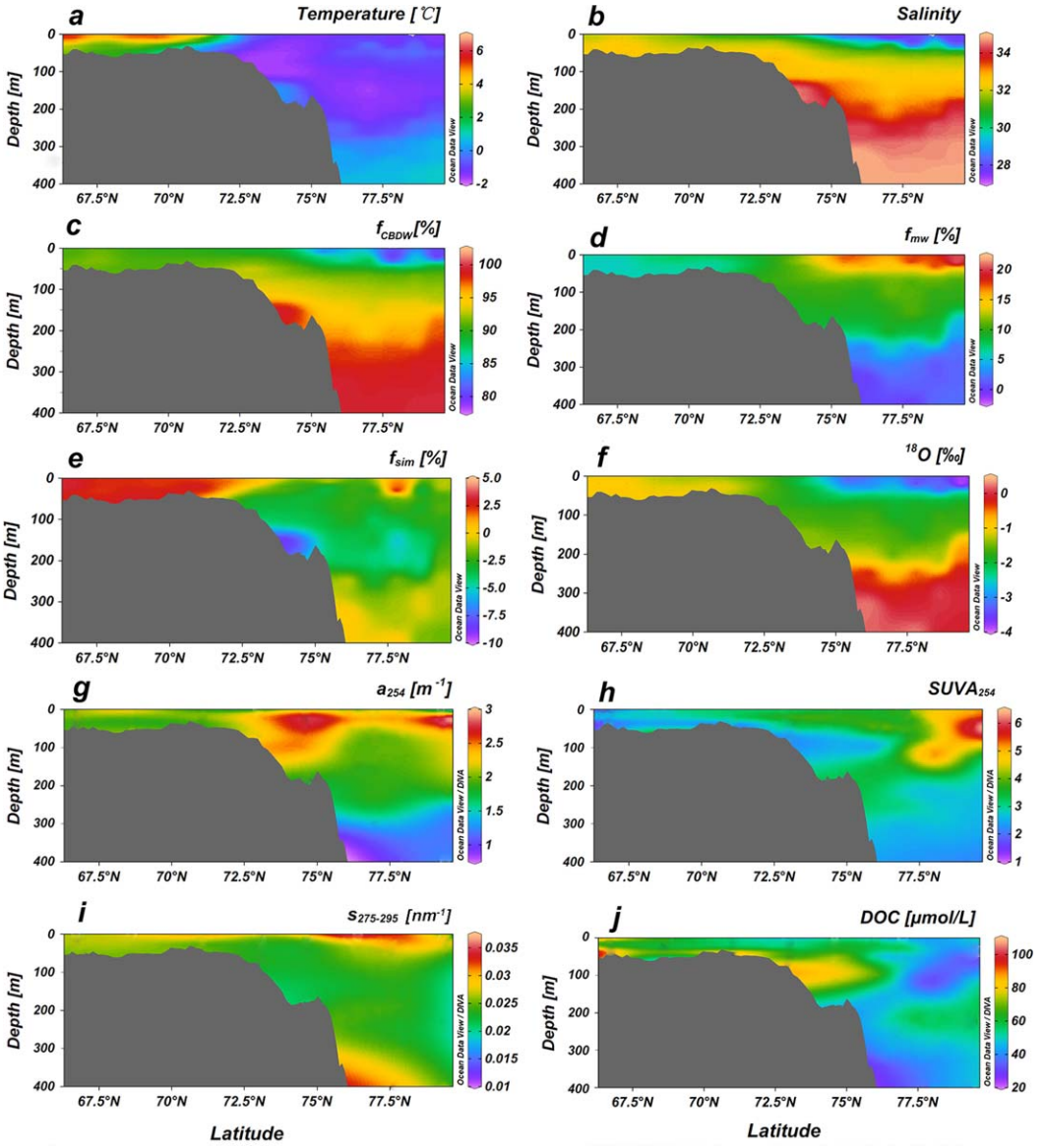

Figure 3. The distribution of (a) temperature (°C), (b) salinity, (c) f_{CBDW} (%), (d) f_{mw} (%), (e) f_{sim} (%), (f) $\delta^{18}O$ (‰), (g) a_{254} (m^{-1}), (h) $SUVA_{254}$ ($m^{-1}/\mu M$), (i) $s_{275-295}$ (nm^{-1}), and (j) DOC (μM) in the upper 400 m water column along Section R in the Chukchi Sea. f_{CBDW}, f_{mw}, and f_{sim} are calculated from mass balance of salinity and $\delta^{18}O$ with a three end-member mixing model.

northern Chukchi Sea (Figure 3h), indicating a high aromaticity. Compared with the low $SUVA_{254}$ observed in the shelf, the high aromaticity in the northern region indicated a strong terrigenous CDOM input from the eastern shelves transported by Transpolar Drift Current [*Guéguen et al.*, 2007; *Stedmon et al.*, 2011].

3.2. CDOM in the Eastern Chukchi Sea (Section S)

Section S, located at the boundary between the eastern Chukchi Shelf and the Beaufort Sea (Figure 1), is influenced by both high primary production in the Chukchi Shelf and terrestrial input from the Mackenzie River [*Walsh et al.*, 1989]. The cold (−1 to −2°C) and fresh (salinity <30) water, occupied the surface layer of the Beaufort Sea, was mainly contributed from the meteoric water (Figures 4a and 4b), supplied from the Mackenzie River and other boreal runoffs [*Guéguen et al.*, 2007]. Thermocline and halocline were observed at a depth of approximate 200 m. This strong stratification prevented the vertical mixing between surface water and deep water (Figures 4a and 4b). The salinity in surface water decreased offshore along the transect (Figure 4b), which is consistent with previous observations [e.g., *Rutgers Van der Loeff et al.*,

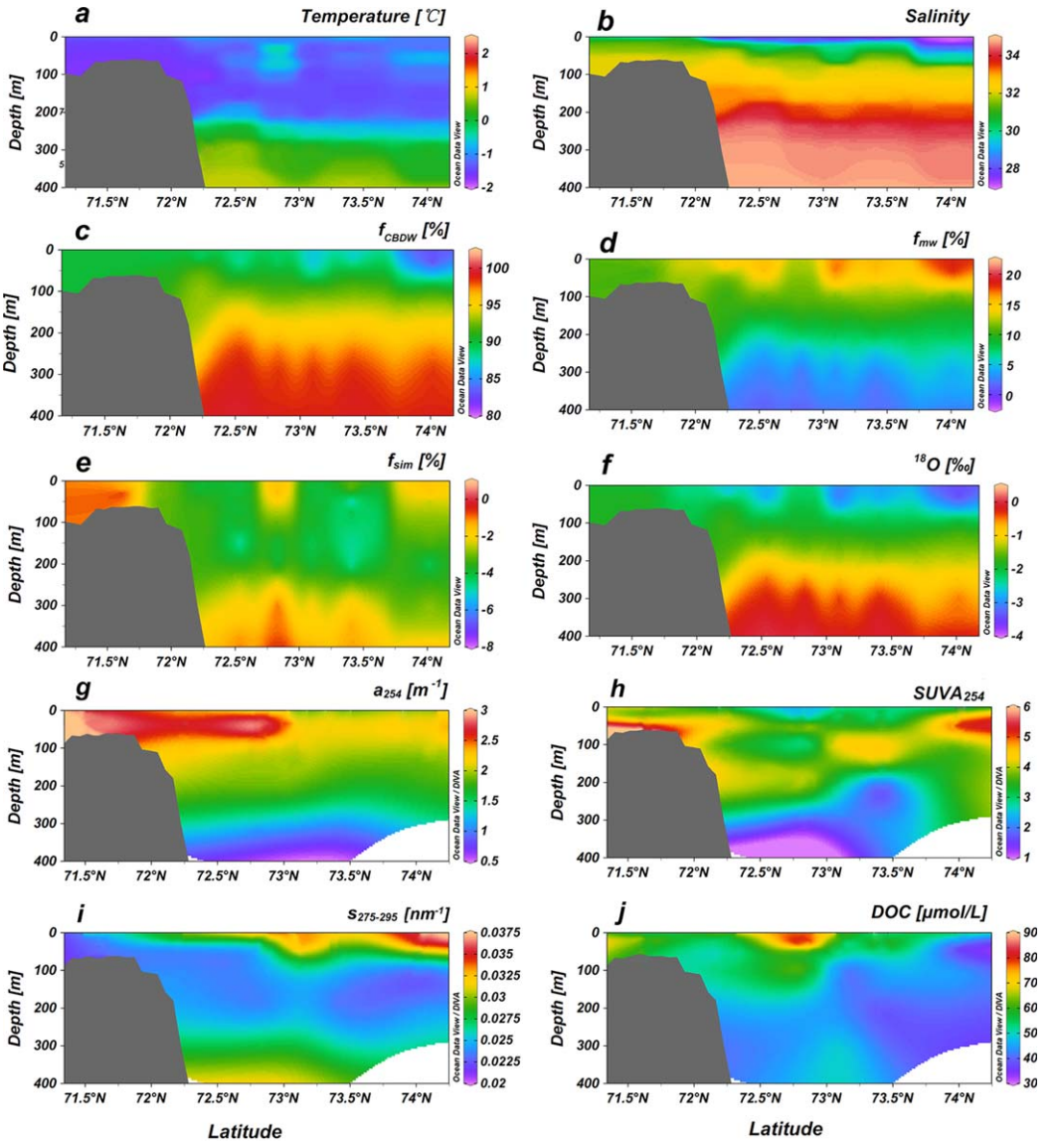

Figure 4. The distribution of (a) temperature (°C), (b) salinity, (c) f_{CBDW} (%), (d) f_{mw} (%), (e) f_{sim} (%), (f) $\delta^{18}O$ (‰), (g) a_{254} (m^{-1}), (h) $SUVA_{254}$ (m^{-1}/μM), (i) $s_{275-295}$ (nm^{-1}), and (j) DOC (μM) in the upper 400 m water column along Section S in the eastern Chukchi Sea. f_{CBDW}, f_{mw}, and f_{sim} are calculated from mass balance of salinity and $\delta^{18}O$ with a three end-member mixing model.

1995; *Kadko and Muench*, 2005]. The f_{mw} values ranged from 0 to 20% (Figure 4d), which agree with earlier estimates of meteoric water in the western Arctic Ocean [*Chen et al*., 2003, 2008; *Pan et al*., 2014; *Tong et al*., 2014].

The sectional distribution of a_{254}, $SUVA_{254}$, DOC, and f_{mw} were analogous to salinity, with the high values occurred in surface water and decreased with increasing depth (Figures 4d, 4g, 4h, and 4j). Consistent with the results reported by *Guéguen et al*. [2007], the high CDOM a_{254} values presented in the thermo-haline (37–125 m), while the f_{sim} and $s_{275-295}$ exhibited low values in the thermo-haline at this section (Figures 4e, 4g, and 4i).

3.3. Size Fractogram of Colloidal Organic Matter

The size distribution of natural colloids in boreal rivers [*Chen et al*., 2004; *Guéguen et al*., 2013] and subtropical coastal water [*Stolpe et al*., 2010, 2013, 2014] have been reported. To the best of our knowledge, no previous studies have reported the size spectrum of colloidal organic matter in the high-latitude Arctic Ocean.

Table 3. The Hydrodynamic Diameter and Molecular Weights of Each Size-Fraction of Colloids Separated by the AF4

Size Fractions	Hydrodynamic Diameter (D_h) (nm)	Molecular Weights (kDa)	References
Small	1.41–3.30	1–10	This study
Medium	3.30–7.74	10–100	
Large	>7.74	>100	
CDOM-colloids	0.5–4	0.061–16.6	*Stolpe et al.* [2010]
Protein-like colloids	3–8	7.73–203.6	

The fractograms of the UV_{254} of colloidal CDOM were composed by three single peaks with the maximum peak (M_p) located within MWs ranging from 1.62 to 2.52 kDa (Table 4 and Figure 5). The M_p range in the Chukchi Shelf is consistent with previous studies [*Stolpe and Hassellöv*, 2007; *Stolpe et al.*, 2010, 2014; *Cuss and Guéguen*, 2012; *Zhou et al.*, 2016]. For example, *Cuss and Guéguen* [2012] found that the microbial humic-like and terrestrial visible humic-like colloidal components in aquatic environments had intermediate size distribution (1.6 ± 0.15 kDa) which is similar with our results, while the terrestrial fulvic-like and tryptophan/polyphenol-like fluorescence had a larger size (4.3 ± 0.66 kDa). *Stolpe et al.* [2010] found that the size distribution of CDOM-colloids ranged from 0.5 to 4 nm, which is at the range of 0.061–16.6 kDa (Table 3). The colloidal CDOM were operationally divided into three different size fractions including the 1–10, 10–100, and >100 kDa. Our results showed that two smaller colloidal fractions (the 1–10 and 10–100 kDa) were the main constituent in the Chukchi Shelf. Their integrated UV_{254} represented 57.4% of the bulk colloids (Table 4). The highest colloidal CDOM UV_{254} was observed in the upper thermo-haline layer (37–125 m) (Figure 5), consistent with the a_{254} (Figure 3g). Lower colloidal CDOM UV_{254} in surface waters might be associated with the strong photolysis effect during Arctic summer, while the high values observed at subsurface layer might result from the condensed brine injection due to the sea ice formation and primary production from sea ice algae in the Chukchi and Beaufort Seas [*Gradinger*, 2009].

4. Discussion

4.1. Variations in Colloidal Size Distribution

Sectional distributions of the integrated UV_{254} of three colloidal fractions are presented in Figure 6. The integrated UV_{254} maximum of three fractions were observed in subsurface layer. However, the 1–10 and 10–100 kDa fractions were latitudinal different with the >100 kDa fraction. The UV_{254} intensities of small (1–10 kDa) and medium colloids (10–100 kDa) in shallow shelf waters (e.g., stations R01, R03, R05, and R07) were lower than those in slope and basin waters, while UV_{254} intensities of the large colloids (>100 kDa) were higher in the Chukchi shelf than in the slope and basin.

The difference in latitudinal distribution between colloidal size fractions would be related to their different sources. *Stolpe et al.* [2013] suggested that the increasing discharge of Yukon River enhanced the export of terrestrial colloidal organic matter (4–40 nm, ~>100 kDa) to the Bering Sea. With the northward movement of Alaska Coastal Current, the large sized colloidal organic matter could be transported to the Chukchi Sea and the western Arctic Ocean. During their transportation, colloids with high molecular weights could be degraded into small colloids by photo-chemical and biological degradation [*Opsahl and Benner*, 1998; *Hernes*, 2003]. Therefore, relative abundance of larger sized colloids was higher in the Chukchi shelf, whereas the small and medium colloids were higher in the slope and basin waters (Figure 6).

4.2. Elevated CDOM in the Thermo-Haline Layer

Both CDOM a_{254} and the integrated UV_{254} of three colloidal size fractions were the highest in the thermo-haline layer (37–125 m) in the Chukchi Sea (Figures 3a, 3b, 3g, and 3h), which is consistent with the SCM in the thermo-haline layer of the western Arctic Ocean [*Seekell et al.*, 2015; *Martini et al.*, 2016]. Higher CDOM in subsurface water compared to surface layer and deep water could result from several physico-chemical and biogeochemical processes, such as sea-ice melt and formation, strong stratification, primary production and mineralization of organic matter, and photo-degradation. Primary production from phytoplankton and injected brine water released from sea-ice formation increased the CDOM concentration in the subsurface layer [*Guéguen et al.*, 2007]. Primary production is one of the most important sources of CDOM and colloidal organic matter in the Chukchi Sea. In addition, part of brine water released from sea-ice formation remained in the thermo-haline layer during summer (Figure 3e). Fractionation process

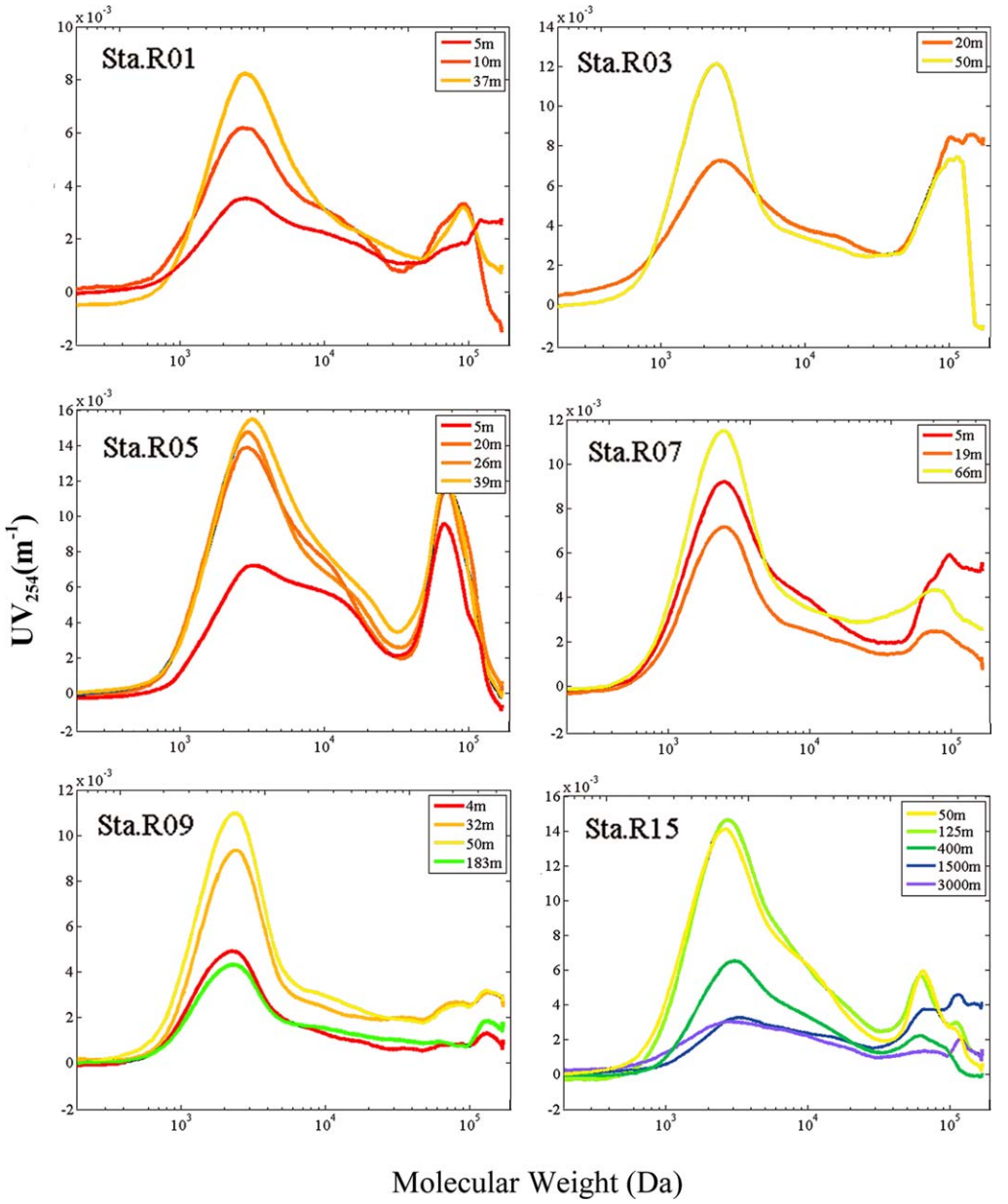

Figure 5. Size fractograms of colloidal CDOM at six stations in the Chukchi Sea. The size spectra of samples from different depths at the same station are presented by different colors.

during sea-ice formation would release some organic matter in brine water, which might cause the high CDOM concentration observed in the thermo-haline in summer [*Hill and Zimmerman*, 2016]. Meanwhile, strong stratification in summer and photo-degradation could reduce CDOM in the surface ocean. The relatively intensive and long sunlight radiation in summer will enhance the degradation of optically active CDOM and colloidal organic components in surface water [*Opsahl and Benner*, 1998; *Reader and Miller*, 2011]. Additionally, sea-ice melted water might dilute CDOM and colloids in the surface water. Fraction of sea-ice melted water in Chukchi Sea surface water is at the range of 0.36–5.30% (Figure 3e). Due to the fractionation during sea-ice formation, CDOM in the sea-ice is relatively low [*Hill and Zimmerman*, 2016]. On the other hand, lower CDOM in the deep water column could be related to the mineralization of DOM and lack of DOM production. Colloids and CDOM could be degraded by bacteria and transformed into small molecules, i.e., CO or CO_2 [*Helms et al.*, 2013], or recalcitrant DOM [*Jiao et al.*, 2010], resulting in a low CDOM in deep water.

Table 4. The Molecular Weights of Size Fractogram Peak (M_p) and the Integrated a_{254} in Each Fractions (1–10, 10–100, and >100 kDa)[a]

			Integrated a_{254} (m^{-1} min)		
Station	Depth (m)	M_p (kDa) (Avg ± SD)	1–10 kDa	10–100 kDa	>100 kDa
R01	5	2.52 ± 0.13	0.60	1.55	3.14
	10	2.10 ± 0.11	0.50	0.56	0.85
	37	2.24 ± 0.11	0.66	1.68	2.06
R03	20	2.24 ± 0.11	1.01	2.50	7.87
	50	1.67 ± 0.08	1.33	1.89	4.51
R05	5	1.97 ± 0.10	0.68	1.28	1.80
	20	2.04 ± 0.10	0.72	1.31	1.83
	26	2.31 ± 0.12	0.73	1.57	1.84
	39	2.45 ± 0.12	0.33	0.99	1.38
R07	5	1.79 ± 0.09	0.79	1.37	1.78
	19	1.79 ± 0.09	0.94	1.65	2.13
	66	1.73 ± 0.09	1.11	1.56	1.52
R09	4	1.56 ± 0.08	0.54	0.95	0.39
	32	1.67 ± 0.08	1.75	3.36	4.04
	50	1.62 ± 0.08	1.19	1.52	1.59
	183	1.51 ± 0.08	0.68	1.04	1.10
R15	50	1.79 ± 0.09	0.89	1.44	1.20
	125	2.45 ± 0.12	0.12	0.39	0.91
	400	1.97 ± 0.10	0.18	0.40	0.41
	1500	2.24 ± 0.11	0.30	0.61	0.35
	3000	1.67 ± 0.08	0.74	1.09	0.89

[a]The M_p is presented in the average (Avg) and standard deviation (SD).

4.3. Source and Fate of CDOM in the Chukchi Sea

The fate and dynamics of CDOM are controlled by several processes in the western Arctic Ocean, such as riverine input, in situ biological production, fractionation during sea ice formation/melting, and release from the resuspended sediments [*Coble*, 2007; *Guéguen et al*., 2007]. Based on our results, we proposed that terrestrial riverine input is more dominant than other processes in controlling the CDOM distribution in the Chukchi Sea. Several lines of evidence presented below would support this statement.

First, the f_{mw} is an indicator of meteoric water, which is predominantly contributed by the river runoff in the western Arctic Ocean [*Ekwurzel et al*., 2001; *Macdonald et al*., 2002; *Mathis et al*., 2007]. Therefore, the f_{mw} is

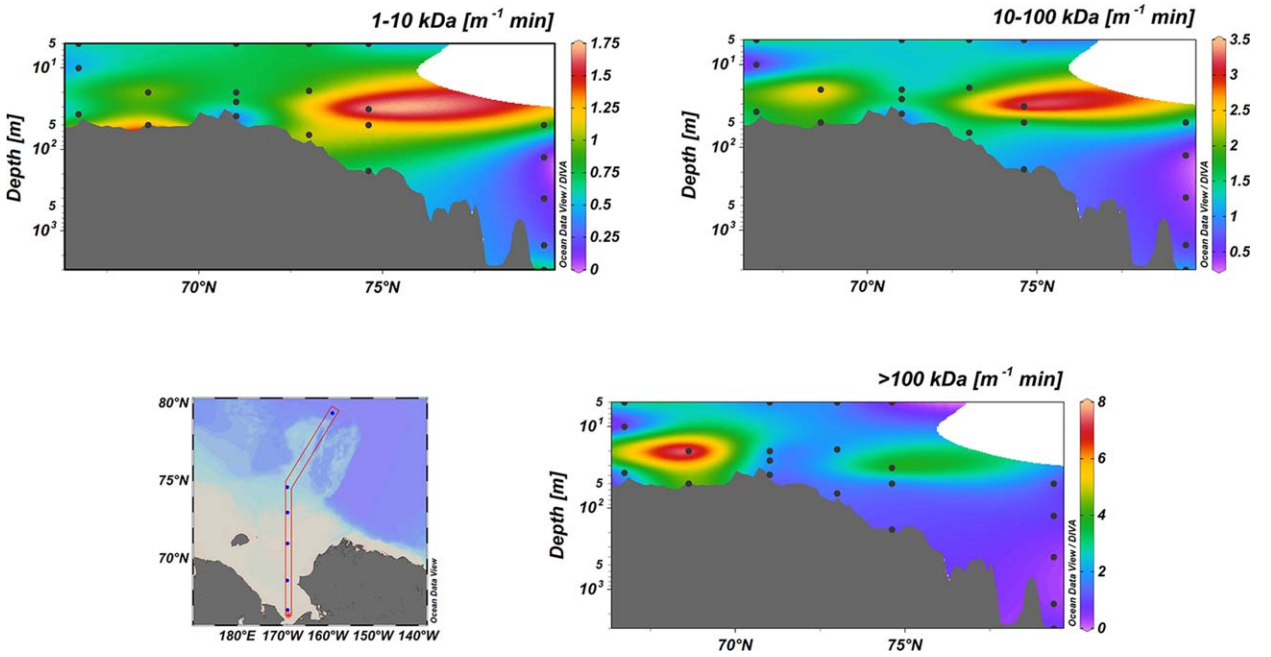

Figure 6. Sectional distribution of the integrated UV_{254} for three size fractions (1–10, 10–100, and >100 kDa) in Section R.

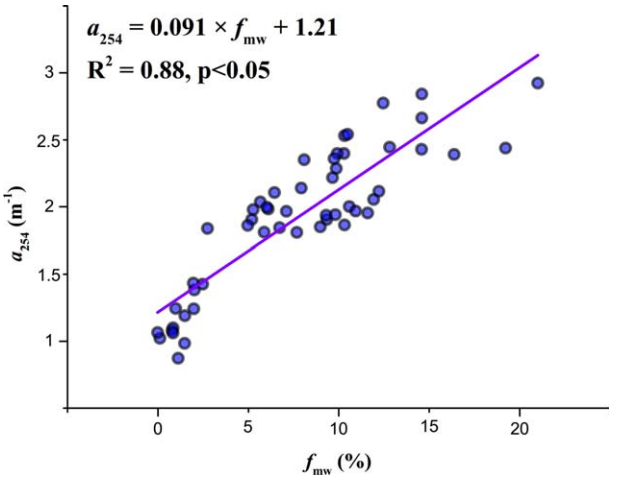

Figure 7. Linear correlation between the f_{mw} (%) and the CDOM a_{254} (m^{-1}) in the Chukchi Sea.

a quantitative proxy for terrestrial CDOM input [*Stedmon et al.*, 2011; *Granskog et al.*, 2012]. Indeed, a robust linear relationship between the f_{mw} and a_{254} ($R^2 = 0.88$, $P < 0.05$) was found in the study area (Figure 7), indicating terrestrial input is a major contributor of bulk CDOM in the Chukchi Sea. Significant relationship between a_{254} and DOC concentration was observed in the Chukchi slope and basin ($R^2 = 0.312$, $P < 0.01$), where the terrestrial input is a main contributor (Figure 3d). In addition, a significant correlation between the integrated intensity of colloidal fractions (including the 1–10, 10–100, and >100 kDa) and the f_{mw} were also observed, indicating colloidal CDOM was mainly derived from terrestrial source (Figure 8). The significance of the correlation between integrated signal intensity and f_{mw} decreased with increasing MW (Figure 8). The strongest correlation ($R^2 = 0.54$, $P < 0.05$) between the f_{mw} and the 1–10 kDa fraction was observed. A empirical relation between molecular weights and hydrodynamic diameter used by several previous studies was used to convert the colloidal molecular weights into the hydrodynamic diameter [*Giddings et al.*, 1976; *Schimpf et al.*, 2005; *Stolpe et al.*, 2010; *Zhou et al.*, 2016]. The colloidal fraction between 1 and 10 kDa corresponded to colloids with a hydrodynamic diameter of 1.41–3.30 nm (Table 3). Obviously, compared to the larger size fractions, the 1–10 kDa colloidal CDOM fraction was highly regulated by terrestrial input. Our results are consistent with those from *Stolpe et al.* [2010]. According to their studies, the CDOM-colloids, whose size ranged from 0.5 to 4 nm, were mainly contributed by terrestrial input, while the 3–8 nm protein-like colloids were derived from autochthonous production [*Stolpe et al.*, 2010].

Although absorption coefficient at wavelengths between 300 and 400 nm is commonly recognized as a terrestrial indicator [*Guéguen et al.*, 2014], measurements of CDOM a_{375} in the Canada Basin exhibit no significantly correlation with the fraction of riverine freshwater [*Stedmon et al.*, 2011]. In contrast to the CDOM a_{375}, a strong correlation between a_{254} and f_{mw} in the Chukchi Shelf was measured, indicating the CDOM a_{254} is a potential indicator of tDOM in the western Arctic Ocean. Likely, different wavelengths could be used to track different DOM components.

Second, although the Chukchi Shelf is considered as a highly productive ecosystem [*Chen et al.*, 1993], there was no significant correlation between primary productivity and CDOM a_{254} during our sampling period, which indicates indirect impacts from in situ biological activities to the CDOM pool in the Chukchi Seas (data not shown). Similarly, no direct relationship between CDOM and *Chl a* was observed in the western Arctic Ocean, pointing to a weak autochthonous CDOM contribution [*Guéguen et al.*, 2007, and reference therein]. On the contrary, a much greater proportion of autochthonous CDOM was observed in the Canada Basin surface water [*Stedmon et al.*, 2011]. In fact, the relationship between the CDOM a_{254} and biological activities might be diminished by additional processes. *Laurion and Mladenov* [2013] suggested that photochemical process transformed the autochthonous DOM from chromophoric components to nonchromophoric species, which could hardly be detected by UV-vis absorbance. *Benner and Amon* [2014] found that photochemical processes accelerate turnover of DOM and degrade the HMW DOM into LMW-DOM. Therefore, under relatively intensive summer sunlight in polar areas, photochemical processes were a significant sink of autochthonous DOM in surface water. Similarly, *Osburn et al.* [2009] suggest that sunlight exposure does not substantially degrade CDOM on Arctic shelves when light attenuation from particle and CDOM-rich river water was considered.

Third, sea ice melting and formation have a limited influence on CDOM pool in the Chukchi Sea. Although the sectional distribution of f_{sim} is similar to that of a_{254} (Figures 3e and 3g), the f_{sim} value in the upper halocline was relatively low, ranging from 2.5 to 5%, which are lower than the f_{mw} in the halocline (10–20%). Low

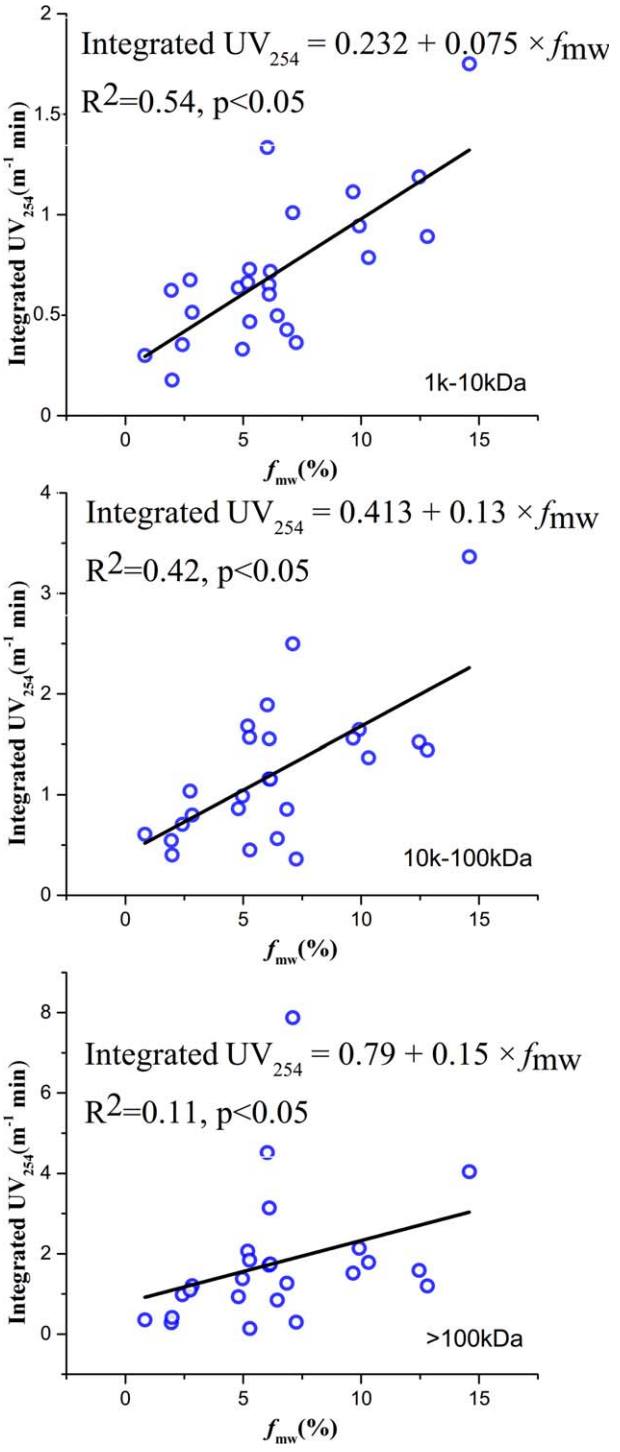

Figure 8. Linear correlation between the integrated UV_{254} (m^{-1} min) of three sized fractions of colloidal CDOM and the f_{mw} (%). The three size fractions of 1–10, 10–100, and >100 kDa were presented from top to bottom, respectively.

proportion of sea-ice melted water will not significantly dilute or change CDOM a_{254}. Besides, brine injection during sea ice formation also have little influence on CDOM. As described in *Guéguen et al.* [2007], the relatively low CDOM in winter-formed brine was resulted from the low riverine input flux during winter to the western Arctic Ocean.

Finally, sediment resuspension has also been reported as a DOM source in the benthic nepheloid layer [*Guo and Santschi*, 2000]. However, our results showed that the maxima of CDOM a_{254} were observed in the thermo-haline, but not the deep layer, which indicated sediment resuspension might have a minor contribution to CDOM signals in the Chukchi Sea.

4.4. Possible Underestimation of Terrestrial Input by Modeled $s_{275–295}$

The optical slope of absorption spectrum, $s_{275–295}$ has been recognized as a proxy for tDOM in aquatic environments. It was first demonstrated that $s_{275–295}$ was a reliable indicator of DOC-normalized yield of dissolved lignin, a terrestrial-derived biomarker [*Opsahl and Benner*, 1997]. Subsequently, $s_{275–295}$ was found to be related to CDOM average MW, DOC-normalized absorption coefficient, percent of terrigenous dissolved organic carbon (%tDOC), and source of DOM in both rivers and coastal oceans [*Helms et al.*, 2008; *Fichot and Benner*, 2011, 2012]. Based on MODIS AQU satellite remote sensing reflectance derived from five different wavelengths and CDOM absorption coefficient spectra, *Fichot and Benner* [2012] proposed a multiple linear regression to model the $s_{275–295}$, which was used to trace tDOM in the Arctic.

Comparisons between modeled and in situ measured $s_{275–295}$ are depicted in Figure 9. A significant correlation between the modeled and measured $s_{275–295}$ was observed ($R^2 = 0.56$ in July and 0.35 in August, Figure 9). However, most of the data were located under the 1:1 reference line. For example, 46% of model-estimated $s_{275–295}$ in July resided within ±10% confidence. However, in August, only 29% model-estimated $s_{275–295}$ were within ±10% confidence. Obviously, the model overestimated the $s_{275–295}$ in our study area, implying that terrestrial input to the Chukchi Sea was underestimated. Actually, recent increase in terrestrial input into the Arctic Ocean has been well

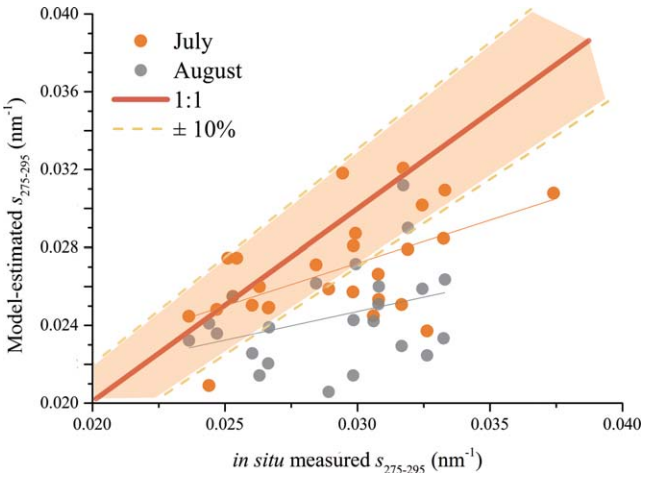

Figure 9. The comparison between in situ measured and model-estimated $s_{275-295}$ in the Chukchi Sea. The red line represents the model-estimated $s_{275-295}$ with ±10% uncertainty. The in situ measured $s_{275-295}$ from July and August in 2014 are presented in orange and grey dots. Note that most of the in situ data were located below the model-estimated, and the slopes of linear regression line in each sampling month are also lower than 1:1.

documented [*Wisser et al.*, 2009; *Shiklomanov and Lammers*, 2011; *Doxaran et al.*, 2015]. Due to warming temperature and changing atmospheric circulation, increased discharge of boreal rivers and the delivery of associated terrestrial materials should have increased tDOM input to the western Arctic Ocean [*Doxaran et al.*, 2015]. Besides, dissolved and particulate organic matter released from the melting permafrost also enlarge tDOM pool in the western Arctic Ocean [*Guo et al.*, 2007]. The increase in tDOM might significantly alter the optical properties of DOM, including their abundance, composition, and distributions in the Arctic Ocean. This would lead to an overestimation of $s_{275-295}$, and thus underestimation of tDOM by the model. Thus, the model proposed by *Fichot and Benner* [2012] might not work well for the Chukchi Sea, and a better optical model for the predication of tDOM is needed.

5. Conclusions

We report here optical properties of CDOM and size fractogram of colloidal CDOM in the Chukchi Sea. The integrated UV_{254} of three colloidal size fractions were highest in the thermo-haline in the Chukchi Sea, similar to the CDOM a_{254}. Both the CDOM a_{254} and UV_{254} of three colloidal fractions (including the 1–10, 10–100, and >100 kDa) showed great correlation with the fraction of meteoric water (f_{mw}), which indicated that the tDOM dominate optical properties of CDOM, and the CDOM a_{254} is a potential tracer for tDOM in the Chukchi Sea. The significance levels of the correlation between the integrated signal intensity and the f_{mw} decreased with increasing molecular weights, suggesting that the smaller colloids (1–10 kDa) was more significantly affected by terrestrial constituents than the larger ones. The larger colloidal fraction (the >100 kDa) was dominant in the Chukchi shelf, while the smaller fractions (1–10 and 10–100 kDa) prevailed in the slope and basin regions. Our in situ measured $s_{275-295}$ was lower than the modeled estimates from *Fichot and Benner* [2012], implying a possible underestimation of tDOM in the Chukchi Sea by the model. Further studies are needed to better understand the dynamics of tDOM and its role in carbon cycles in the Arctic Ocean in a changing climate.

Acknowledgments

The authors would like to thank the two reviewers for their insightful comments and suggestions that have contributed to improve this paper. Thanks also go to Hsuan-Ching Ho and Hengxiang Deng for sampling and Lina Lin for providing CTD data. All data are available from the authors upon request (mchen@xmu.edu.cn). This work was supported, in part, by a Public Science and Technology Research Funds Projects of Ocean (201505034), a Polar Environment Investigation and Assessment supported by Chinese Arctic and Antarctic Administration (CHINARE2016-03-04-03 and CHINARE2016-04-03-05), and a Chinese Natural Science Foundation (41125020).

References

Amon, R. M. W., et al. (2012), Dissolved organic matter sources in large Arctic rivers, *Geochim. Cosmochim. Acta*, *94*, 217–237, doi:10.1016/j.gca.2012.07.015.

Baalousha, M., B. Stolpe, and J. R. Lead (2011), Flow field-flow fractionation for the analysis and characterization of natural colloids and manufactured nanoparticles in environmental systems: A critical review, *J. Chromatogr. A*, *1218*(27), 4078–4103, doi:10.1016/j.chroma.2011.04.063.

Bauch, D., M. R. van der Loeff, N. Anderson, S. Torres-Valdes, K. Bakker, and E. P. Abrahamsen (2011), Origin of freshwater and polynya water in the Arctic Ocean halocline in summer 2007 Dorothea, *Prog. Oceanogr.*, *49*, 1–37, doi:10.1016/j.pocean.2011.1007.1017.

Benner, R. (2004), Export of young terrigenous dissolved organic carbon from rivers to the Arctic Ocean, *Geophys. Res. Lett.*, *31*, L05305, doi:10.1029/2003GL019251.

Benner, R., and R. M. W. Amon (2014), The size-reactivity continuum of major bioelements in the ocean, *Annu. Rev. Mar. Sci.*, *7*, 185–205, doi:10.1146/annurev-marine-010213-135126.

Benner, R., P. Louchouarn, and R. M. W. Amon (2005), Terrigenous dissolved organic matter in the Arctic Ocean and its transport to surface and deep waters of the North Atlantic, *Global Biogeochem. Cycles*, *19*, GB2025, doi:10.1029/2004GB002398.

Chen, C.-T. A., K.-K. Liu, and R. W. Macdonald (1993), Continental margin exchanges, in *Ocean Biogeochemistry: The Role of the Ocean Carbon Cycle in Global Change*, edited by M. J. R. Fasham, pp. 53–97, Springer, Berlin.

Chen, M., Y. Huang, J. Mingming, and Y. Qiu (2003), The sources of the upper and lower halocline water in the Canada Basin derived from isotopic tracers, *Sci. China Ser. D*, *46*(6), 625–639, doi:10.1360/03yd9055.

Chen, M., N. Xing, Y. Huang, and Y. Qiu (2008), The mean residence time of river water in the Canada Basin, *Chin. Sci. Bull.*, *53*(5), 777–783, doi:10.1007/s11434-008-0077-z.

Chen, R. F., P. Bissett, P. Coble, R. Conmy, G. B. Gardner, M. A. Moran, X. Wang, M. L. Wells, P. Whelan, and R. G. Zepp (2004), Chromophoric dissolved organic matter (CDOM) source characterization in the Louisiana Bight, *Mar. Chem.*, *89*(1–4), 257–272, doi:10.1016/j.marchem.2004.03.017.

Coble, P. G. (2007), Marine optical biogeochemistry: The chemistry of ocean color, *Chem. Rev.*, *107*, 402–418.

Coble, P. G., J. Lead, A. Baker, D. Reynolds, and R. G. M. Spencer (2014), *Aquatic Organic Matter Fluorescence*, edited by P. G. Coble, et al., Cambridge Univ. Press, Cambridge, U. K.

Cuss, C. W., and C. Guéguen (2012), Determination of relative molecular weights of fluorescent components in dissolved organic matter using asymmetrical flow field-flow fractionation and parallel factor analysis, *Anal. Chim. Acta*, *733*, 98–102, doi:10.1016/j.aca.2012.05.003.

Dai, M., Z. Yin, F. Meng, Q. Liu, and W.-J. Cai (2012), Spatial distribution of riverine DOC inputs to the ocean: an updated global synthesis, *Curr. Opin. Environ. Sustainability*, *4*(2), 170–178, doi:10.1016/j.cosust.2012.03.003.

Doxaran, D., E. Devred, and M. Babin (2015), A 50% increase in the mass of terrestrial particles delivered by the Mackenzie River into the Beaufort Sea (Canadian Arctic Ocean) over the last 10 years, *Biogeosciences*, *12*(11), 3551–3565, doi:10.5194/bg-12-3551-2015.

Dubascoux, S., F. Von Der Kammer, I. Le Hécho, M. P. Gautier, and G. Lespes (2008), Optimisation of asymmetrical flow field flow fractionation for environmental nanoparticles separation, *J. Chromatogr. A*, *1206*(2), 160–165, doi:10.1016/j.chroma.2008.07.032.

Ekwurzel, B., P. Schlosser, R. A. Mortlock, R. G. Fairbanks, and J. H. Swift (2001), River runoff, sea ice meltwater, and Pacific water distribution and mean residence times in the Arctic Ocean, *J. Geophys. Res.*, *106*(C5), 9075–9092, doi:10.1029/1999JC000024.

Fichot, C. G., and R. Benner (2011), A novel method to estimate DOC concentrations from CDOM absorption coefficients in coastal waters, *Geophys. Res. Lett.*, *38*, L03610, doi:10.1029/2010GL046152.

Fichot, C. G., and R. Benner (2012), The spectral slope coefficient of chromophoric dissolved organic matter ($S_{275\text{-}295}$) as a tracer of terrigenous dissolved organic carbon in river-influenced ocean margins, *Limnol. Oceanogr.*, *57*(5), 1453–1466, doi:10.4319/lo.2012.57.5.1453.

Fichot, C. G., K. Kaiser, S. B. Hooker, R. M. W. Amon, M. Babin, S. Bélanger, S. A. Walker, and R. Benner (2013), Pan-Arctic distributions of continental runoff in the Arctic Ocean, *Sci. Rep.*, *3*, 1053, doi:10.1038/srep01053.

Giddings, J. C. (1993), Field-flow fractionation : Analysis of macromolecular, colloidal, and particulate materials, *Science*, *260*(5113), 1456–1465.

Giddings, J. C. (1995), Measuring colloidal and macromolecular properties by FFF, *Anal. Chem.*, *67*(19), 592A–598A.

Giddings, J. C., F. J. F. Yang, and M. N. Myers (1976), Flow field-flow fractionation : A versatile new separation method, *Science*, *193*(4259), 1244–1245.

Gradinger, R. (2009), Sea-ice algae: major contributors to primary production and algal biomass in the Chukchi and Beaufort Seas during May/June 2002, *Deep Sea Res., Part II*, *56*(17), 1201–1212, doi:10.1016/j.dsr2.2008.10.016.

Granskog, M. A., C. A. Stedmon, P. A. Dodd, R. M. W. Amon, A. K. Pavlov, L. De Steur, and E. Hansen (2012), Characteristics of colored dissolved organic matter (CDOM) in the Arctic outflow in the Fram Strait: Assessing the changes and fate of terrigenous CDOM in the Arctic Ocean, *J. Geophys. Res.*, *117*, C12021, doi:10.1029/2012JC008075.

Guay, K. C., G. P. Klinkhammer, K. K. Kenison, P. G. Coble, T. E. Whitledge, F. J. Bussell, and T. A. Wagner (1999), High-resolution measurements of dissolved organic carbon in the Arctic Ocean by in situ fiber-optic spectrometry, *Geophys. Res. Lett.*, *26*(8), 1007–1010.

Guéguen, C., L. Guo, M. Yamamoto-Kawai, and N. Tanaka (2007), Colored dissolved organic matter dynamics across the shelf-basin interface in the western Arctic Ocean, *J. Geophys. Res.*, *112*, C05038, doi:10.1029/2006JC003584.

Guéguen, C., C. W. Cuss, and W. Chen (2013), Asymmetrical flow field-flow fractionation and excitation-emission matrix spectroscopy combined with parallel factor analyses of riverine dissolved organic matter isolated by tangential flow ultrafiltration, *Int. J. Environ. Anal. Chem.*, *93*, 1428–1440, doi:10.1080/03067319.2013.764415.

Guéguen, C., C. W. Cuss, C. J. Cassels, and E. C. Carmack (2014), Absorption and fluorescence of dissolved organic matter in the waters of the Canadian Artic Archiipelago, Baffin Bay, and the Labrador Sea, *J. Geophys. Res. Ocean.*, *119*, 2034–2047, doi:10.1002/2013JC009173.

Guo, L., and P. H. Santschi (2000), Sedimentary sources of old high molecular weight dissolved organic carbon from the ocean margin benthic nepheloid layer, *Geochim. Cosmochim. Acta*, *64*(4), 651–660, doi:10.1016/S0016-7037(99)00335-X.

Guo, L., C. H. Coleman, and P. H. Santschi (1994), The distribution of colloidal and dissolved organic carbon in the Gulf of Mexico, *Mar. Chem.*, *45*, 105–119.

Guo, L., C. L. Ping, and R. W. Macdonald (2007), Mobilization pathways of organic carbon from permafrost to arctic rivers in a changing climate, *Geophys. Res. Lett.*, *34*, L13603, doi:10.1029/2007GL030689.

Hansell, D. A., D. Kadko, and N. R. Bates (2004), Degradation of terrigenous dissolved organic carbon in the western Arctic Ocean, *Science*, *304*(5672), 858–861, doi:10.1126/science.1096175.

Helms, J. R., A. Stubbins, J. D. Ritchie, E. C. Minor, D. J. Kieber, and K. Mopper (2008), Absorption spectral slopes and slope ratios as indicators of molecular weight, source, and photobleaching of chromophoric dissolved organic matter, *Limnol. Oceanogr.*, *53*(3), 955–969, doi:10.4319/lo.2008.53.3.0955.

Helms, J. R., A. Stubbins, E. M. Perdue, N. W. Green, H. Chen, and K. Mopper (2013), Photochemical bleaching of oceanic dissolved organic matter and its effect on absorption spectral slope and fluorescence, *Mar. Chem.*, *155*, 81–91, doi:10.1016/j.marchem.2013.05.015.

Hernes, P. J. (2003), Photochemical and microbial degradation of dissolved lignin phenols: Implications for the fate of terrigenous dissolved organic matter in marine environments, *J. Geophys. Res.*, *108*(C9), 3291, doi:10.1029/2002JC001421.

Hill, V. J., and R. C. Zimmerman (2016), Characteristics of colored dissolved organic material in first year landfast sea ice and the underlying water column in the Canadian Arctic in the early spring, *Mar. Chem.*, *180*, 1–13, doi:10.1016/j.marchem.2016.01.007.

Jackson, J. M., H. Melling, J. V. Lukovich, D. Fissel, and D. G. Barber (2015), Formation of winter water on the Canadian Beaufort shelf: New insight from observations during 2009-2011, *J. Geophys. Res. Ocean*, *120*, 4090–4107, doi:10.1002/2015JC010812.

Jiao, N., et al. (2010), Microbial production of recalcitrant dissolved organic matter: long-term carbon storage in the global ocean, *Nat. Rev. Microbiol.*, *8*(8), 593–599, doi:10.1038/nrmicro2386.

Kadko, D., and R. Muench (2005), Evaluation of shelf-basin interaction in the western Arctic by use of short-lived radium isotopes: The importance of mesoscale processes, *Deep Sea Res., Part II*, *52*(24–26), 3227–3244, doi:10.1016/j.dsr2.2005.10.008.

Laurion, I., and N. Mladenov (2013), Dissolved organic matter photolysis in Canadian arctic thaw ponds, *Environ. Res. Lett.*, *8*(3), 035026, doi:10.1088/1748-9326/8/3/035026.

Letscher, R. T., D. A. Hansell, and D. Kadko (2011), Rapid removal of terrigenous dissolved organic carbon over the Eurasian shelves of the Arctic Ocean, *Mar. Chem.*, *123*(1–4), 78–87, doi:10.1016/j.marchem.2010.10.002.

Macdonald, R. W., F. A. Mclaughlin, and E. C. Carmack (2002), Fresh water and its sources during the SHEBA drift in the Canada Basin of the Arctic Ocean, *Deep Sea Res., Part I*, *49*, 1769–1785.

Mangal, V., and C. Guéguen (2015), Examining concentrations and molecular weights of thiols in microorganism cultures and in Churchill River (Manitoba) using a fluorescent-labeling method coupled to asymmetrical flow field-flow fractionation, *Anal. Bioanal. Chem.*, *407*, 4305–4313, doi:10.1007/s00216-015-8599-0.

Martini, K. I., P. J. Stabeno, C. Ladd, P. Winsor, T. J. Weingartner, C. W. Mordy, and L. B. Eisner (2016), Dependence of subsurface chlorophyll on seasonal water masses in the Chukchi Sea, *J. Geophys. Res. Ocean*, *121*, 1755–1770, doi:10.1002/2015JC011359.

Mathis, J. T., R. S. Pickart, D. A. Hansell, D. Kadko, and N. R. Bates (2007), Eddy transport of organic carbon and nutrients from the Chukchi Shelf: Impact on the upper halocline of the western Arctic Ocean, *J. Geophys. Res.*, *112*, C05011, doi:10.1029/2006JC003899.

Opsahl, S., and R. Benner (1997), Distribution and cycling of terrigenous dissolved organic matter in the ocean, *Nature*, *386*(6624), 480–482, doi:10.1038/386480a0.

Opsahl, S., and R. Benner (1998), Photochemical reactivity of dissolved lignin in river and ocean waters, *Limnol. Oceanogr.*, *43*(6), 1297–1304, doi:10.4319/lo.1998.43.6.1297.

Osburn, C. L., L. Retamal, and W. F. Vincent (2009), Photoreactivity of chromophoric dissolved organic matter transported by the Mackenzie River to the Beaufort Sea, *Mar. Chem.*, *115*(1), 10–20.

Pan, H., M. Chen, J. Tong, Y. Qiu, M. Zheng, and J. Cao (2014), Variation of freshwater components in the Canada Basin during 1967–2010, *Acta Oceanol. Sin.*, *33*(6), 40–45, doi:10.1007/s13131-014-0487-5.

Reader, H. E., and W. L. Miller (2011), Effect of estimations of ultraviolet absorption spectra of chromophoric dissolved organic matter on the uncertainty of photochemical production calculations, *J. Geophys. Res.*, *116*, C08002, doi:10.1029/2010JC006823.

Rutgers van der Loeff, M. M., R. M. Key, J. Scholten, D. Bauch, and A. Michel (1995), ^{228}Ra as a tracer for shelf water in the Arctic Ocean, *Deep Sea Res., Part II*, *42*(6), 1533–1553, doi:10.1016/0967-0645(95)00053-4.

Saito, T., T. Hamamoto, T. Mizuno, T. Iwatsuki, and S. Tanaka (2015), Comparative study of granitic and sedimentary groundwater colloids by flow-field flow fractionation coupled with ICP-MS, *J. Anal. At. Spectrom.*, *30*(6), 1229–1236, doi:10.1039/C5JA00088B.

Schimpf, M. E., K. Caldwell, and J. C. Giddings (2005), *Field-Flow Fractionation Handbook*, Wiley-Interscience, 537 pp., John Wiley, N. Y.

Seekell, D. A., J.-F. Lapierre, J. Ask, A.-K. Bergström, A. Deininger, P. Rodríguez, and J. Karlsson (2015), The influence of dissolved organic carbon on primary production in northern lakes, *Limnol. Oceanogr.*, *60*(4), 1276–1285, doi:10.1002/lno.10096.

Shiklomanov, A. I., and R. B. Lammers (2011), River discharge, in *Arctic Report Card: Update for 2011: Tracking Recent Environmental Changes*, Institute for the Study of Earth, Oceans, and Space, University of New Hampshire, Durham. [Available at http://www.arctic.noaa.gov/report11/river_discharge.html.]

Stedmon, C. A., and S. Markager (2001), The optics of chromophoric dissolved organic matter (CDOM) in the Greenland Sea: An algorithm for differentiation between marine and terrestrially derived organic matter, *Limnol. Oceanogr.*, *46*(8), 2087–2093, doi:10.4319/lo.2001.46.8.2087.

Stedmon, C. A., R. M. W. Amon, A. J. Rinehart, and S. A. Walker (2011), The supply and characteristics of colored dissolved organic matter (CDOM) in the Arctic Ocean: Pan Arctic trends and differences, *Mar. Chem.*, *124*(1–4), 108–118, doi:10.1016/j.marchem.2010.12.007.

Steig, E. J., V. Gkinis, A. J. Schauer, S. W. Schoenemann, K. Samek, J. Hoffnagle, K. J. Dennis, and S. M. Tan (2014), Calibrated high-precision ^{17}O-excess measurements using cavity ring-down spectroscopy with laser-current-tuned cavity resonance, *Atmos. Meas. Tech.*, *7*(8), 2421–2435, doi:10.5194/amt-7-2421-2014.

Stolpe, B., and M. Hassellöv (2007), Changes in size distribution of fresh water nanoscale colloidal matter and associated elements on mixing with seawater, *Geochim. Cosmochim. Acta*, *71*(13), 3292–3301, doi:10.1016/j.gca.2007.04.025.

Stolpe, B., L. Guo, A. M. Shiller, and M. Hassellöv (2010), Size and composition of colloidal organic matter and trace elements in the Mississippi River, Pearl River and the northern Gulf of Mexico, as characterized by flow field-flow fractionation, *Mar. Chem.*, *118*(3–4), 119–128, doi:10.1016/j.marchem.2009.11.007.

Stolpe, B., L. Guo, and A. M. Shiller (2013), Binding and transport of rare earth elements by organic and iron-rich nanocolloids in Alaskan rivers, as revealed by field-flow fractionation and ICP-MS, *Geochim. Cosmochim. Acta*, *106*, 446–462, doi:10.1016/j.gca.2012.12.033.

Stolpe, B., Z. Zhou, L. Guo, and A. M. Shiller (2014), Colloidal size distribution of humic- and protein-like fluorescent organic matter in the northern Gulf of Mexico, *Mar. Chem.*, *164*, 25–37, doi:10.1016/j.marchem.2014.05.007.

Tong, J. (2014), The freshwater balance derived from oxygen isotopes in the western Arctic Ocean, PhD thesis, Coll. of Ocean and Earth Sci., Xiamen Univ., Xiamen, China.

Tong, J., M. Chen, Y. Qiu, Y. Li, and J. Cao (2014), Contrasting patterns of river runoff and sea-ice melted water in the Canada Basin, *Acta Oceanol. Sin*, *33*(6), 46–52, doi:10.1007/s13131-014-0488-4.

Wahlund, K. G., and J. C. Giddings (1987), Properties of an asymmetrical flow field-flow fractionation channel having one permeable wall, *Anal. Chem.*, *59*(9), 1332–1339.

Walker, S. A., R. M. W. Amon, C. A. Stedmon, S. Duan, and P. Louchouarn (2009), The use of PARAFAC modeling to trace terrestrial dissolved organic matter and fingerprint water masses in coastal Canadian Arctic surface waters, *J. Geophys. Res.*, *114*, G00F06, doi:10.1029/2009JG000990.

Walsh, J. J., et al. (1989), Carbon and nitrogen cycling within the Bering/Chukchi Seas: Source regions for organic matter effecting AOU demands of the Arctic Ocean, *Prog. Oceanogr.*, *22*(4), 277–359, doi:10.1016/0079-6611(89)90006-2.

Weingartner, T., K. Aagaard, R. Woodgate, S. Danielson, Y. Sasaki, and D. Cavalieri (2005), Circulation on the north central Chukchi Sea shelf, *Deep Sea Res., Part II*, *52*(24–26), 3150–3174, doi:10.1016/j.dsr2.2005.10.015.

Weishaar, J. L., G. R. Aiken, B. A. Bergamaschi, M. S. Fram, R. Fujii, and K. Mopper (2003), Evaluation of specific ultraviolet absorbance as an indicator of the chemical composition and reactivity of dissolved organic carbon, *Environ. Sci. Technol.*, *37*(20), 4702–4708, doi:10.1021/es030360x.

Wisser, D., B. M. Fekete, C. J. Vörösmarty, and A. H. Schumann (2009), Reconstructing 20th century global hydrography: A contribution to the Global Terrestrial Network- Hydrology (GTN-H), *Hydrol. Earth Syst. Sci. Discuss.*, *6*(2), 2679–2732, doi:10.5194/hessd-6-2679-2009.

Zhou, Z., and L. Guo (2015), A critical evaluation of an asymmetrical flow field-flow fractionation system for colloidal size characterization of natural organic matter, *J. Chromatogr. A*, *1399*, 53–64.

Zhou, Z., B. Stolpe, L. Guo, and A. M. Shiller (2016), Colloidal size spectra, composition and estuarine mixing behavior of DOM in river and estuarine waters of the northern Gulf of Mexico, *Geochim. Cosmochim. Acta*, *181*, 1–17, doi:10.1016/j.gca.2016.02.032.